Dynamic decomposition of aliphatic molecules on Al(111) from *ab initio* molecular dynamics

Jun Zhong
School of Materials, Arizona State University, Tempe, Arizona 85287-8706, USA

Louis G. Hector, Jr.
Materials and Processes Laboratory, General Motor R&D Center, Warren, Michigan 48090-9055, USA

James B. Adams
School of Materials, Arizona State University, Tempe, Arizona 85287-8706, USA

(Received 4 October 2008; revised manuscript received 21 December 2008; published 19 March 2009)

Ab initio molecular dynamics based on density functional theory within the generalized gradient approximation was used to explore decomposition on Al(111) of butanol-alcohol and butanoic-acid, two important boundary additives in Al processing. Each molecule was oriented with its functional group closest to the surface and then given an initial velocity toward the surface. Decomposition occurred upon collision with Al(111) resulting in the formation of adhered fragments that represent the very initial stages in additive film formation during plastic deformation where nascent Al is liberated. Bonding interactions over the simulation time frames were explored with contours of the electron localization function. Results of the simulations were compared with existing experimental studies of chemical decomposition on clean Al surfaces and found to be in qualitative accord. The effects of other initial molecular orientations on decomposition were explored in ancillary calculations where the molecules were rotated through 90° and 180° prior to collision with Al(111).

DOI: 10.1103/PhysRevB.79.125419 PACS number(s): 71.15.Pd, 61.82.Pv, 68.43.Fg, 79.20.Rf

I. INTRODUCTION

Molecular interaction with solid surfaces has attracted considerable attention in the scientific literature due its relevance to such areas as catalysis,[1] atmospheric pollution,[2] magnetic storage systems,[3] planetary science,[4] organic electronic materials,[5] soil contamination,[6] molecular information processing,[7] and geophysics.[8] Theoretical studies have often focused on model systems designed to explore adsorption of a single aliphatic or aromatic molecule. Common practice is to probe energetics of surface reactions by either manually moving a molecule from surface site to surface site, or removing specific atoms in order to induce bonding with surface ions. For example, Lee *et al.*[9] reported a first-principles investigation of C_2H_2 decomposition on Fe(001), while Dyson and Smith used an empirical interatomic potential to investigate chemisorption of C_2H_2 and CH_3 on β-SiC(001).[10] An empirical density functional method was developed in Ref. 11 to model adsorption of several molecules on Si(100) including C_6H_6 and $C_{10}H_8$. Experimental studies of molecule-solid interactions have involved a variety of surface science methodologies.[12] For example, Xie *et al.*[13] investigated CH_3OH dissociation on Si(111)-(7×7) with scanning tunneling microscopy (STM). Land *et al.*[14] also used STM to explore C_2H_4 reaction on Pt(111), and inelastic electron-tunneling spectroscopy has been applied to the study of carboxylic acid reaction with alumina.[15,16]

Dynamic molecular decomposition, which results from collision of molecules with a solid surface, has received minimal attention in the literature. An especially important example is the decomposition of boundary additive molecules on a reactive metal surface. Nowhere is this more relevant than in various Al forming processes such as rolling, forging, casting, machining, and extrusion where boundary additive molecules facilitate a series of complex reactions leading to molecularly thin boundary films that adhere to the Al surface. These technologically and economically critical processes are often the first in a series of steps that ultimately result in a wide range of Al alloy components used in the commercial and military sectors. Common additives consist of one or more aliphatic alcohols, acids or esters with hydroxyl (O-H) and carboxyl (O=C-OH) groups, respectively.[17,18] These electron-rich functional groups react with nascent Al once the natural 3–6 nm Al oxide or hydroxide layer is broken up during plastic deformation. The adhered boundary films limit adhesive transfer and abrasive wear, lower interface temperatures, and mitigate energy input required to plastically deform the material.[19] In the absence of these films, contact with oxide surfaces on ferrous tools can produce a highly exothermic (thermit) reaction: $2Al+Fe_2O_3\rightarrow Al_2O_3+2Fe$; alternatively, similar thermit reactions can promote adhesive transfer and subsequent Al surface damage.[20] Reactions that lead to adsorbed boundary additives are typically inferred from expensive trial-and-error experimentation and it is upon these inferences that additive molecules are often synthesized.

Several experimental investigations of aliphatic molecule interactions with clean Al surfaces suggest a chemical reactivity with Al that differs significantly from that of transition-metal surfaces. For example, adsorption and thermal decomposition of H_2O, CH_3OH, and CH_3OCH_3 molecules on clean Al(111) were examined in Refs 21–24. High-resolution electron energy-loss spectroscopy (HR-EELS), temperature programmed desorption (TPD), and Auger-electron spectroscopy (AES) were used to investigate molecular adsorption on the Al surface. At 90 K, these molecules retarded surface oxidization. Above 90 K, decomposition species from these molecules on Al(111) were observed. Although such reactions have been well studied, there continues to be some uncertainty about decomposition species on Al during reac-

tion. Underhill and Timsit[25] applied x-ray photoelectron spectroscopy (XPS) to the investigation of 1-butanol and propanoic-acid decomposition on Al(111). Their results (at room temperature) suggest that acid molecules break up on clean Al surface leading to attachment of aliphatic chain fragments via C atoms. Alternatively, aliphatic alcohols were found to chemisorb on clean Al via the functional group alone. At elevated temperatures, both acids and alcohols dissociated on the clean surface via their functional groups.

Computer simulations of boundary film formation on metallic surfaces have primarily focused on extreme pressure additives that minimize wear and corrosion of reciprocating contacts where no bulk plastic deformation occurs. An additive of particular interest is zinc-dialkyl-dithiophosphate (ZDDP) which decomposes to form high strength boundary films that adhere to iron and steel surfaces.[26,27] Using Car-Parinello molecular dynamics, Mosey *et al.*[28] predicted that ZDDP boundary films form by cross linking through the Zn atoms once a certain pressure is reached within the film. The pressures required for cross linking are mitigated by the mechanical properties of the substrate. While ZDDP films form on Al surfaces, they do not effectively inhibit wear on these softer surfaces to anywhere near the extent they do on iron-based surfaces. The molecular dynamics predictions were validated in subsequent experiments.[29] Koyama *et al.*[30] used a hybrid tight-binding method to model interactions between phosphoric ester and nascent iron surface and noted both ionic and covalent bonding. Yim *et al.*[31] used molecular dynamics to explore sliding at an interface between two Si(001) surfaces containing dodecane films. Greenfield and Ohatani[32] modeled friction modifying molecules constrained between two surfaces.

Despite the broad significance of Al alloys, there are relatively few theoretical studies of additive molecule decomposition on a clean Al surface and the resulting structures of molecularly adsorbed species. Most of these studies have focused on reaction of small organic molecules, such as methanol and ethanol, with various Al surface terminations.[33–36] For larger molecule reactions with clean Al surface, Zhong and Adams[37] calculated the reaction enthalpies of vinyl-phosphonic-acid (VPA) and ethanoic-acid (EA) with clean Al(111) in several adsorbing geometries, viz., tribridged, bibridged, and unidentate coordinations. A similar investigation was reported by Hector *et al.*[38] for VPA reaction on α-Al_2O_3(0001). They concluded that these reactions occurred at hydrophosphoryl-oxygen (OH-P=O) groups on VPA, and hydrocarboxyl (OH-C=O) groups on EA. The most favorable adsorption pathway was the tribridged coordination for VPA (which is consistent with vibrational spectroscopy experiments) and the bibridged coordination for EA. Unidentate coordination was found to be the least favorable. At present, there are no dynamic *ab initio* studies that explore large alkyl-chain (e.g., greater than ten ions) dissociation and binding to Al surfaces.

In this paper, we examine dynamic reaction pathways for decomposition and adsorption of two important aliphatic boundary additive chemistries on clean Al(111) surface. Specifically, interactions of single butanol-alcohol and butanoic-acid molecules with Al(111) are modeled using *ab initio* molecular dynamics (monolayer formation on metal surfaces and associated film cohesion are reserved for a forthcoming study) based upon density functional theory (DFT). Each molecule was directed to collide with clean Al(111) surface through its reactive functional group. Initial molecular approach speeds toward the surface were taken from technologically relevant Al forming processes. Bonding both within each molecule and between the molecular fragments and Al(111) is explored in detail with contours of the electron localization function. Simulation results are qualitatively compared with reported x-ray photoelectron spectroscopy (XPS) and electron energy-loss spectroscopy (EELS) experiments of similar molecules.[24,25] The calculations suggest new decomposition species that were not observed in a previous DFT study of static decomposition.[37] To explore the effect of initial molecular orientation on decomposition, ancillary calculations were conducted in which each molecule was either aligned with its carbon backbone parallel to Al(111) or rotated such that its functional group was pointing away from Al(111).

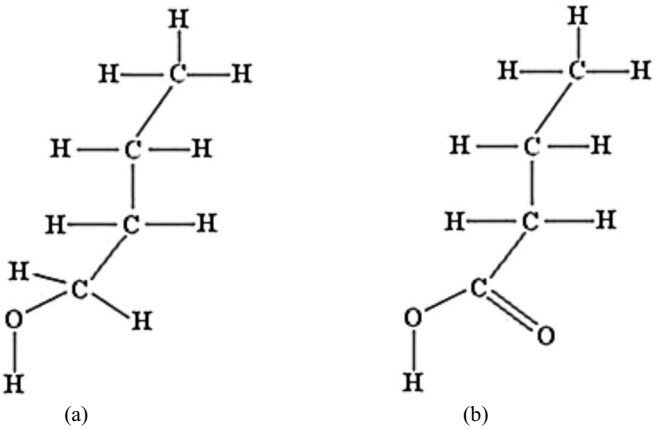

FIG. 1. (a) butanol-alcohol molecule, $[H_3C\text{-}(CH_2)_2\text{-}H_2COH]$. (b) butanoic-acid molecule, $[H_3C\text{-}(CH_2)_2\text{-}COOH]$

II. ADDITIVE MOLECULES

Butanol-alcohol $[H_3C\text{-}(CH_2)_2\text{-}H_2COH]$ and butanoic-acid $[H_3C\text{-}(CH_2)_2\text{-}COOH]$ molecules are shown schematically in Fig. 1. The alcohol in Fig. 1(a) has a C-OH functional group, while the acid in Fig. 1(b) has an O=C-OH functional group with C-OH and C=O groups. Table I lists some relevant bond energies. The Al-O bond strength is highest of all bond strengths listed due to the high electronegativity difference between Al and O.[39] Therefore, oxygen-containing functional groups (i.e., O=C-OH and C-OH) on these molecules will be more reactive to clean Al(111) than hydrocarbon (C-H) groups. This suggests that of all possible initial molecular orientations relative to the surface, that with the func-

TABLE I. Bond energies of some relevant atomic bonds (Ref. 39).

Atomic bond	Al-O	Al-C	Al-H	C-H	C-O	O-H
Bond energy (eV)	5.20	2.77	2.95	4.11	3.71	4.76

tional group closest to the surface is of most interest for simulation of decomposition upon impact. We chose the Al(111) termination since this is the low surface energy termination.[40]

III. COMPUTATIONAL METHODOLOGY

All *ab initio* molecular dynamics (AIMD) calculations in this study were based on DFT (Refs. 41–45) as implemented in the Vienna *ab initio* simulation package (VASP) within a (high precision) plane-wave basis set.[46,47] Vanderbilt-type ultrasoft pseudopotentials (USP) (Ref. 48) were used for the elemental constituents within the generalized gradient approximation (GGA).[49–51] Although the GGA tends to be better than LDA for describing transition states during chemical reactions, its application to molecular adsorption or decomposition problems comes with two significant caveats. First, it is well known that the GGA can yield inaccurate reaction barriers (~10 kJ/mol).[52–54] Second, for small molecules such as CO, the GGA has been shown to overestimate adsorption energies as well as lead to erroneous conclusions about surface adsorption sites.[55] While the semilocal BLYP and hybrid B3LYP functionals accurately predict adsorption energies and correctly distinguish adsorption sites that are consistent with experiment, metallic property and surface energy predictions are typically inaccurate.[55] One is thus faced with a dilemma regarding the choice of exchange-correlation functional for simulation of molecular decomposition on a metallic surface. For dynamic decomposition, our main interest here, we believe that the GGA is a reasonable compromise since the high velocity applied to the molecules (which in practice are heated in upward of 160 °C in bulk Al forming processes such as rolling) and the extreme chemical reactivity of nascent Al will likely overwhelm any barrier to decomposition.

We first calculated the lattice constant of pure Al bulk using an NPT ensemble in AIMD, which thermally equilibrated the system at room temperature (300 K) and an ambient pressure of 1.0 bar. A regular gamma-centered grid of $5\times5\times5$ was chosen as the best k-point sampling for one $2a\times2a\times2a$ unit cell where a is our computed lattice constant for bulk Al. The total energy was converged within 1–2 meV/atom. A plane-wave cutoff energy of 400 eV, as dictated by the oxygen pseudopotential, i.e., the hardest in the decomposition simulations, was adopted for all calculations. The computed lattice constant of 4.05(7) Å compares favorably with results from other calculations and experiment as detailed in Table II.

For modeling interactions between additive molecules and an Al(111) slab, a Monkhorst-Pack grid of $5\times5\times1$ k-points was selected. The Al(111) slab consisted of a supercell geometry with four-Al layers (36 ions per layer or 144 ions in the entire slab). This orthorhombic supercell has three definite orientations, viz., $a[1\bar{1}0]=14.88$ Å (along the X axis), $b[11\bar{2}]=17.18$ Å (along the Y axis,) and $c[111]=40.00$ Å (along the Z axis), with a vacuum distance of 24.00 Å in the c direction. The supercell size was sufficient so as to preclude interactions with periodic images. The bottom layer of the Al(111) slab was fixed along the c direction to prevent motion of the slab during impact with an additive molecule. Ancillary tests with thicker Al(111) slabs revealed no significant differences from results computed with the four-layer slab. A check of the magnitude of the topmost layer relaxations revealed that these were less than 2% of the bulk lattice spacing which is in agreement with Ref. 40. The geometries of the isolated molecules were first optimized in the same supercell as that used for the Al(111) slab, but with Al ions removed. Each optimization was conducted with a single k point using the Fermi smearing technique.[46,47] The optimized molecules were then transferred into the simulation cell containing the Al(111) slab.

TABLE II. Comparison of calculated lattice constant of pure Al bulk (unit: Å).

Current AIMD work at 300 K	DFT work at 0 K[a]	EAM-MD work at 300 K[b]	Experimental data at 300 K[c]
4.05(7)	4.05(3)	4.05	4.05

[a]Reference 37.
[b]Reference 56.
[c]Reference 57.

A simulation time step of 0.001 ps was chosen to ensure computational efficiency while minimizing integration errors. For example, during a typical MD simulation at 500 time steps, the total energy of the system changed by less than 0.03 eV.

At the beginning of each simulation, the additive molecule under study and the four-layer Al(111) slab were equilibrated in the same cell at 300 K for about 1500 time steps (1 time step=0.001 ps). This was maintained by rescaling the velocities at each time step.[58] After thermal equilibration, all AIMD simulations were carried out with the constant energy method (the no temperature control energy molecular dynamics ensemble).

When steel rollers converge to form the bite region in metal rolling of Al alloys, pressure gradients that develop in applied liquid lubricant films draw them into the conjunction. After collision of a steel roller surface with additive molecules, we estimate that translational speeds acting on a single molecule can reach as high as 2500 m/s due to kinematics at the tool/Al interface.[59] Hence, a set of approach velocities, $\boldsymbol{V}_d$, based upon this value, were selected for investigation in the AIMD simulations. Each molecule then starts to accelerate once it feels a net attraction of the Al(111) slab.

To save computational cost, the initial vertical distance between each additive molecule and Al(111) surface ions was set to 2.30 Å. This distance was relative to one or more of the functional group ions in each molecule and is in fact slightly larger than the Al-O bond length (1.86–1.97 Å) in Ref. 60.

To provide insight into the nature of bonding interactions between additive molecule fragments and Al(111) from dynamic decomposition, we compute and display contours of the electron localization function (ELF) in planes where bonding is expected to occur based upon the optimized decomposition geometries. As discussed by Räsänen *et al.*[61] in

their work on quantum dots, the ELF describes where electrons are localized rather than where they are. From a more formal standpoint, the ELF represents the probability of finding a second electron, e^-, with the same spin in the neighboring region of a reference electron.[62–64] Additional details about the ELF and its relationship to the concept of the Fermi hole and the Pauli exclusion principle may be found in Ref. 65. Values of the ELF are restricted to $0.0 \leq \mathrm{ELF} \leq 1.0$, with 0.5 representing electron-gas-like pair probability (e.g., as in crystalline Al, which is a free-electron gas metal) and 1.0, which indicates localization (i.e., covalent bonding, as in crystalline diamond). The ELF has proven useful for investigating bonding between two neighboring ions since contour lobes that are representative of localized charge (or overlapping orbitals) can be clearly distinguished from lobes that are indicative of minimal charge localization. We note that ELF has provided insights into bonding in a variety of organic molecules,[66–72] inorganic compounds,[40,73] and in solid-solid adhesion.[74,75] Specific advantages and some intrinsic limitations of the ELF have been reviewed by Savin.[40,76]

IV. MODEL CONFIGURATIONS

Figure 2 shows four initial model configurations explored with the present AIMD simulations. In each model, the additive molecule is positioned with its carbon backbone above the center of the equilibrated Al(111) slab surface. Molecular orientations along $[11\bar{2}]$ [or side views, Figs. 2(a), 2(c), 2(e), and 2(g)] and [111] (or top-down views, Figs. 2(b), 2(d), 2(f), and 2(h)] are shown. In each top-down view, most of the hydrocarbon backbone has been removed to reveal the alignment of the functional group relative to the surface plane. Ion colors are red (O), black (C), white (H), or gray (Al), and the ball-and-stick displays are merely suggestive of bonding between ions. The Al(111) slab surface is slightly nonplanar at the outset of each AIMD simulation due to thermal equilibration at 300 K prior to each additive decomposition simulation. The three model configurations for butanoic-acid decomposition on the Al(111) slab are displayed in Figs. 2(a)–2(f). Figures 2(a) and 2(b) show two views of model-1 (M-1), where $V_d = -15.0$ Å/ps (1500 m/sec). Here the O ion in O=C is set at a 2.30 Å distance above the Al(111) slab. In model-2 (M-2), which is shown in Figs. 2(c) and 2(d), $V_d = -15.0$ Å/ps and the H-O group is positioned at a 2.30 Å above the Al(111) slab. Figures 2(e) and 2(f) show model-3 (M-3) where $V_d = -20.0$ Å/ps and functional group components are positioned 2.30 Å directly above Al(111). Figures 2(g) and 2(h) are views of model-4 (M-4) for butanol-alcohol reaction with the Al(111) slab. Here, the H-O group is positioned 2.30 Å above Al(111). For M-4, $V_d = -20.0$ Å/ps.

V. RESULTS AND DISCUSSION

A. Boundary additive molecules

Figure 3 shows side views of the two additive molecules (before decomposition) with superimposed contours of the electron localization function. The contour planes in Figs. 3(a) and 3(b) were positioned to cut through the center of the carbon backbone in each case.

Figure 3(a) shows ELF contours of an isolated butanol-alcohol molecule following VASP optimization in a cell of sufficient size so as to isolate the molecule from periodic images. Covalent bonds in the carbon backbone are denoted by the oval-shaped red-orange lobes between adjacent C ions at ELF values between 0.9 and 1.0 as denoted in the key to the right of the contour plots. ELF contours about the O ion suggest sp^3 hybridization with the associated H and C ions and significant distortion due to the H ion. Table III shows that our computed C-O-H bond angle of 112.2° in the butanol-alcohol molecule is close to the 109.6° experimental value. Reasonable agreement between our computed O-C and O-H bond lengths and experiment is also noted in Table III. The C ion in CH_3 [top end of the butanol-alcohol molecule, as shown in Fig. 3(a)] is sp^3 hybridized with about 25% s character. Portions of the sp^3 bond cannot be seen since two of the H ions are not coplanar with the C ion and hence their corresponding ELF contours are not displayed.

Figure 3(b) shows ELF contours of an isolated butanoic-acid molecule. Here the O-C single bond is shorter than that in the alcohol, as confirmed by our calculation, and is due to the sp^2 hybridization of the carboxyl C ion in O=C-OH. This has a higher percentage of s character (~33%) than the C in CH_3 of the alcohol which is consistent with a shorter bond distance. The sp^2 hybridization of the C ion in O=C-OH allows electrons to delocalize resulting in the large elliptically shaped orange-red ELF lobe surrounding most of the O ion in O=C. Covalent bonds in the carbon backbone are again denoted by the oval-shaped red-orange lobes between adjacent C ions. Comparisons of additional bond distances and angles from our calculations with experiment are also listed in Table III. The ELF contours in Fig. 3 show that the functional groups (O=C-OH and C-OH) on the additive molecules are electron-rich and hence are more likely to react with Al(111) than other C-H and C-C groups.

B. Decomposition pathways for butanoic-acid

Figures 4–6 show the computed dynamical decomposition pathways for butanoic-acid on the Al(111) slab from models M-1, M-2, and M-3, respectively (see Fig. 2). The initial temperature for the simulations was 300 K, and the cell boundaries have been removed for the purpose of illustration. Only that portion of the surface where the molecules interact is shown in each figure. In all figures, O ions are red, C ions are gray, and H ions are white.

In Fig. 4(a), the O ion in the O=C group in the undissociated butanoic-acid molecule begins to anchor to the surface in a bidentate coordination at 50 simulation time steps. However, the O-H group does not appear to interact with the surface. At 90 time steps, Fig. 4(b) shows that the O ion in O=C has dissociated from the molecule and is adsorbed onto the surface, with the residual molecule anchoring to the surface through its alkyl-chain. In Fig. 4(c), the O-H group has dissociated from the molecular fragment at 200 time steps. This group begins interacting with the surface through its O ion, as expected. At 310 time steps, the O-H group fully

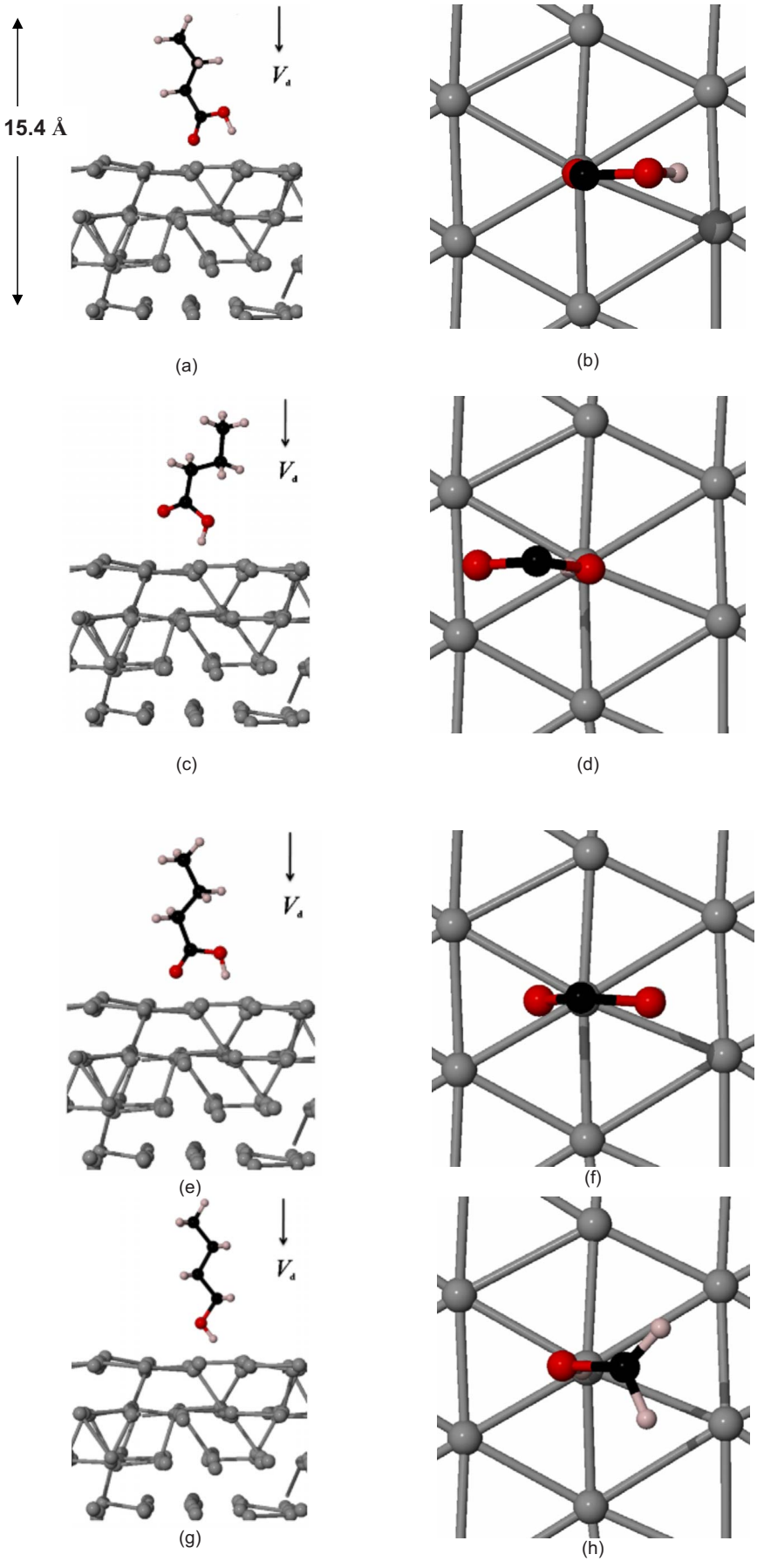

FIG. 2. (Color online) Molecule orientations relative to Al(111) at the outset of the simulations shown along $[11\bar{2}]$ (side view) and [111] (top-down view). The majority of the hydrocarbon backbone has been removed in the top-down views to show functional group alignment relative to the center of the surface plane. Normal velocity imposed to each molecule is $\mathbf{V}_d$. [(a) and (b)] side and top-down views, respectively, of M-1 with butanoic-acid; [(c) and (d)] side and top-down views, respectively, of M-2 with butanoic-acid; [(e) and (f)] side and top-down views, respectively, of M-3 with butanoic-acid; (g),(h) side and top-down views, respectively, of M-4 with butanol-alcohol. Ion colors are red (O), black (C), white (H), and gray (Al). Note that the cell boundaries have been removed for the purpose of display.

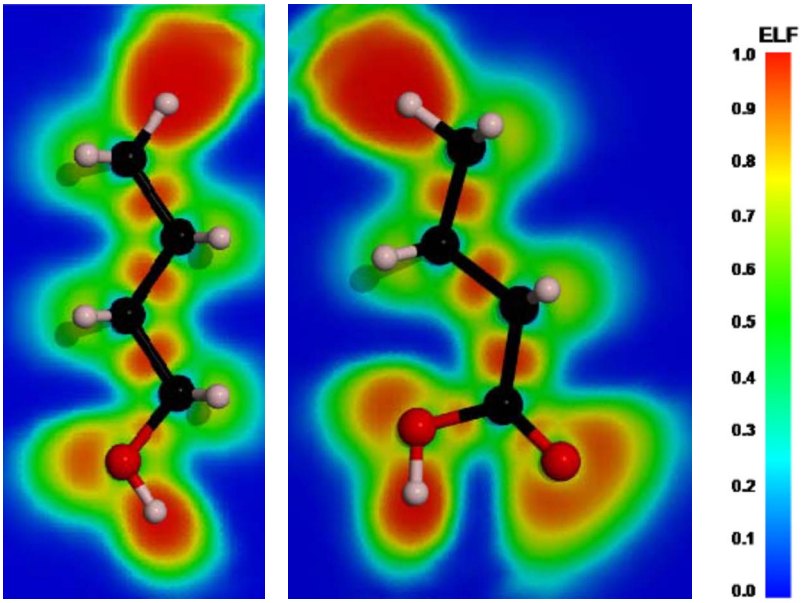

FIG. 3. (Color online) Contours of the electron localization function shown in a single plane that cuts through the carbon backbone of (a) a butanol-alcohol molecule; (b) a butanoic-acid molecule. The H ion at the very top and bottom of each molecule is in the same plane as the carbon back bone, while remaining H ions point in and out of the page. Ion colors are red (O), black (C), and white (H).

dissociates and is adsorbed onto the surface, as shown in Fig. 4(d), in a unidentate coordination. The residual alkyl-chain anchors to the surface in a tetracoordination via the carboxyl C ion, with the O ion in O=C adsorbing on the surface in tridentate coordination. We note that the H ion in the O-H group is tilted relative to the O ion as expected.[80] Also, the decomposition species noted at the four time steps in Fig. 4 were obtained when the calculation was repeated multiple times (with minor changes to the orientations of the various decomposition species). Note that the temperature of this system increases from 300 to 970 K during the simulation.

In Fig. 5(a), which is the M-2 configuration at 40 time steps, the O-H group interacts with Al(111), resulting in dissociation of the H ion from the molecule. The butanoic-acid fragment interacts with the Al surface in a bibridged coordination through its O ions. At 130 time steps, Fig. 5(b) shows that the molecular fragment remains anchored to the surface as shown in Fig. 5(a). At 200 time steps, however, Fig. 5(c) shows this coordination is changing to unidentate as the molecule rebounds following collision with the surface, with an Al ion pulled upward by one of the O ions in the fragment. At 310 time steps, a bidentate configuration results, as shown in Fig. 5(d), which resembles a soap (i.e., a product of *R*-COOM, where *R*- is the alkyl-chain and *M* is a metal ion) formed on the surface.[81] Soap formation with fatty acids has been observed in Al forming processes where nominal pressures are in the vicinity of 2.5 times the material flow strength.[19,66,82] The temperature of this system increased from 300 to 960 K during the simulation.

Results for M-3 in Fig. 6(a) show that the O ion in O=C has dissociated and is subsequently adsorbed in a tridentate configuration on the Al surface at 50 time steps. The same is true for the O-H group. The residual alkyl-chain forms a bidentate configuration. Interestingly, the remaining images at 90, 200, and 310 time steps in Figs. 6(b)–6(d), respectively, suggest that this bidentate configuration persists (once formed) throughout the simulation. The H dissociates from the adsorbed O-H group and migrates about the surface. The temperature of this system increased from 300 to 1330 K during the simulation.

Figure 7 shows the initial evolution of potential energy computed for each of the three butanoic-acid decomposition models considered in Fig. 2. In each case, the butanoic-acid molecule interacts with the surface within 30–40 time steps.

TABLE III. Important geometric parameters of gas-phase molecules.

Butanol-alcohol molecule						Butanoic-acid molecule					
Bond length (Å)			Bond angle (deg.)			Bond length (Å)			Bond angle (deg.)		
Bond	Calc.	Expt.[a]	Angle	Calc.	Expt.[a]	Bond	Calc.	Expt.	Angle	Calc.	Expt.[b]
O-C	1.437	1.404	C-O-H	112.2	109.6	O=C	1.213	1.231[b]	O=C-O	120.1	123.9
						O-C	1.341	1.304[b]			
O-H	0.938	0.947				O-H	0.982	0.964[c]	C-O-H	113.7	117.0

[a]Reference 77.
[b]Reference 78.
[c]Reference 79.

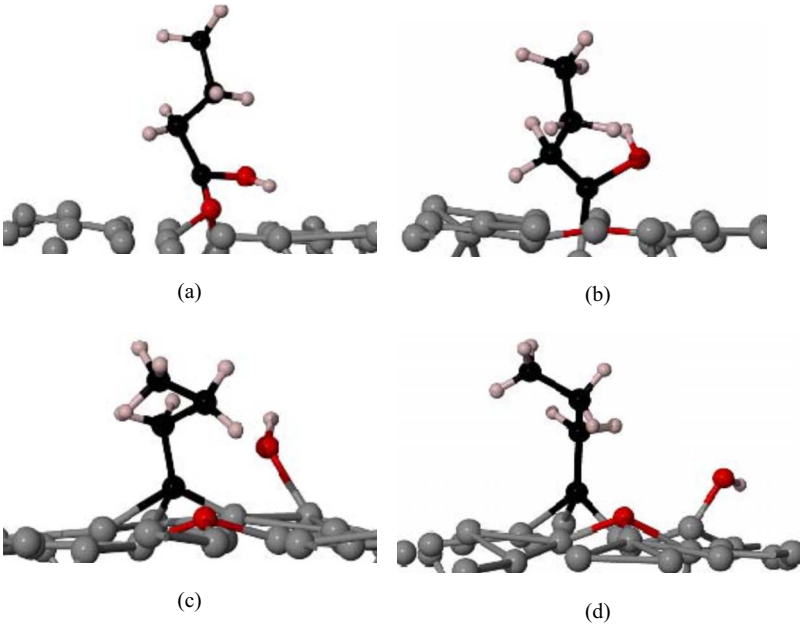

FIG. 4. (Color online) Selected stages of dynamic decomposition pathway for butanoic-acid on Al(111) with initial geometry M-1. (a) 50 steps; (b) 90 steps; (c) 200 steps; (d) 310 steps. Ion colors are red (O), black (C), white (H), and gray (Al).

The potential energy of the system decreases during this time in order to overcome the barrier to adsorption. The energy then decreases (which is the dip in each curve) as the surface absorbs the impact of the molecule which continues to decompose. Beyond this point, the energy once again increases as the molecular fragment and its decomposed functional group components rearrange themselves on the surface. The sharp peaks on the M-1 and M-3 curves indicate larger and more rapid exchanges between the potential and kinetic energies than are observed in M-2 during decomposition. We find that the nominal potential energy for M-1 after 500 time steps is lower than those for M-2 and M-3 suggesting that this is the most energetically stable of the three model configurations. Further annealing of each model configuration is discussed below.

C. Decomposition pathway for butanol-alcohol

Since butanol-alcohol has only one functional group (O-H), we constructed a single model (M-4) to explore its interaction with the Al(111) slab during AIMD simulation. Figure 8 shows four selected time steps during decomposition of the M-4 configuration detailed in the side and top-down views in Figs. 2(g) and 2(h), respectively, starting at 300 K. At 40 time steps, the H ion dissociates from the O-H group and interacts with an Al surface ion in Fig. 8(a). At 100 time steps in Fig. 8(b), the molecular fragment adsorbs on the surface with the lone H ion moving below the surface, albeit only briefly. At 250 time steps, the molecule changes its adsorption geometry to a bidentate structure, as shown in Fig. 8(c). Figure 8(d) shows a unidentate configuration at 400

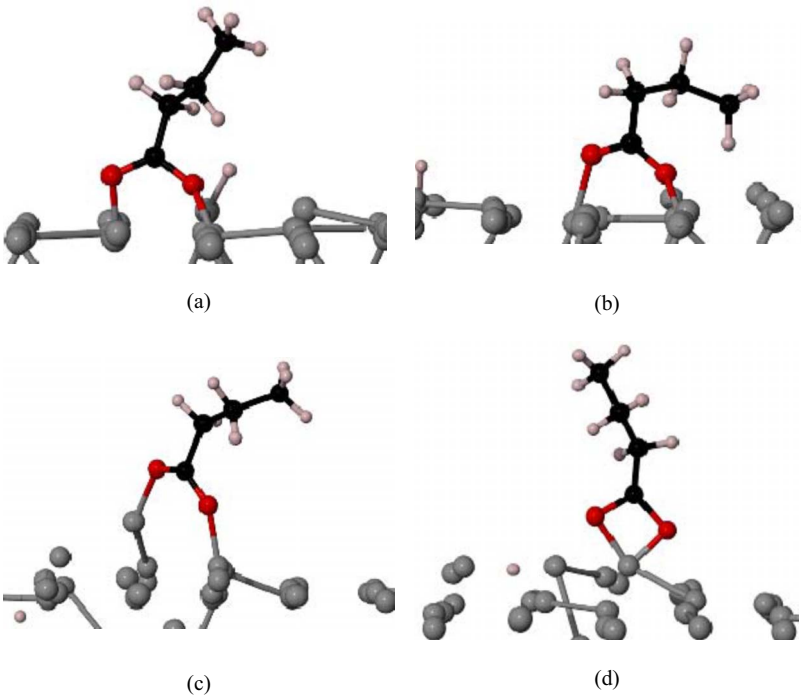

FIG. 5. (Color online) Selected stages of dynamic decomposition pathway for butanoic-acid on Al(111) with initial geometry M-2. (a) 40 steps; (b) 130 steps; (c) 200 steps; (d) 310 steps. Ion colors are red (O), black (C), white (H), and gray (Al).

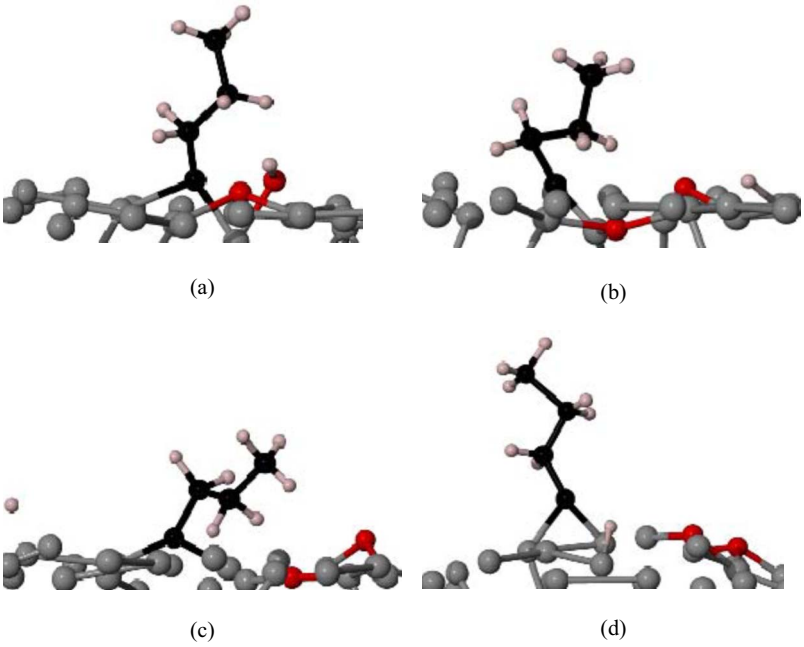

FIG. 6. (Color online) Selected stages of dynamic decomposition pathway for butanoic-acid on Al(111) with initial geometry M-3. (a) 50 steps; (b) 90 steps; (c) 200 steps; (d) 310 steps. Ion colors are red (O), black (C), white (H), gray (Al).

time steps. Interestingly, neither the bidentate nor the tridentate coordinations noted in the butanoic-acid decomposition were observed for butanol-alcohol. Additional AIMD tests with the butanol-alcohol molecule slightly rotated relative to the Al(111) slab confirmed this observation. The temperature of this system ranged from 300–1150 K during AIMD simulation.

Figure 9 shows the potential energy computed during butanol-alcohol decomposition in M-4. Here, the sharp peak around 40 time steps represents dissociation of the H ion from the molecule. The dip in the curve near 220 time steps is due to rearrangement of the decomposed species on the surface.

D. Qualitative comparison of simulation predictions with experiments

Controlled experimental investigation of molecular decomposition on clean Al(111) is challenging from the standpoint that it is difficult to prevent oxidation of the surface even under ultrahigh-vacuum conditions.[83] Underhill and Timsit[25] examined interactions of some aliphatic additives that are very similar to butanoic-acid and butanol-alcohol with clean Al(111) using x-ray photoelectron spectroscopy (XPS). The temperature range in their experiments was 300–750 K. For the acids at 300–500 K, the hydrocarboxylic (O=C-OH) groups decomposed, resulting in two possible decomposition configurations. One configuration involved separation of the O-H group from the original molecule to bind to the surface via the O ion plus the attachment of the residual alkyl-chain to the Al surface via the O ion in O=C. This is the essential pathway of M-1 in Fig. 4(a) which was found to be the most energetically stable of the three butanoic-acid decomposition pathways explored in Figs. 4–6. In the other, the O was completely liberated from the O=C-OH group, locally oxidizing Al(111). The remaining alkyl-chain anchored to the surface via the carboxyl C ion originally in the hydrocarboxyl (O=C-OH) group. This decomposition pathway resulted in the configuration suggested at 200 steps in Fig. 6(c), which is model M-3.

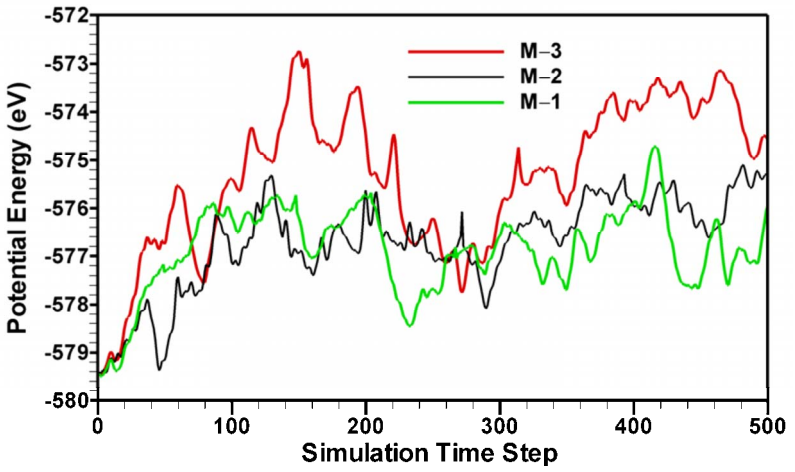

FIG. 7. (Color online) Potential energies with simulation time step for butanoic-acid decomposition on Al(111). Results for M-1, M-2, and M-3 are compared.

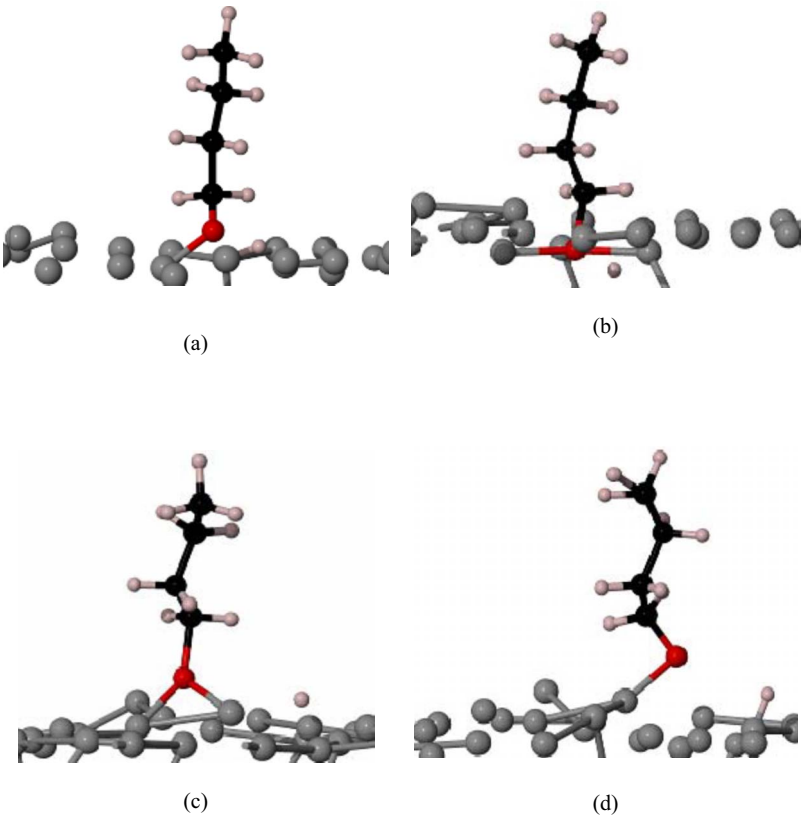

FIG. 8. (Color online) Dynamic decomposition pathway for butanol-alcohol on Al(111) at selected time steps. Initial geometry is M-4 starting at 300 K. (a) 40 steps; (b) 100 steps; (c) 250 steps; (d) 400 steps. Ion colors are red (O), black (C), white (H), and gray (Al).

Crowell *et al.*[21] used electron energy-loss spectroscopy, temperature programmed desorption, and Auger-electron spectroscopy to study adsorption and decomposition of ethanoic acid on A1(111). At 167 K, they found that the adsorbed acetate fully decomposed resulting in a carbon- and oxygen-covered surface. Although the present AIMD simulations were conducted at far shorter length scales than the experiments in Ref. 20, it is likely that with a longer simulation time that the results for single butanoic-acid molecule decomposition would suggest further decomposition of the bound species.

To further corroborate our simulations with these experimental observations, we carried out annealing AIMD simulations[58] equilibrated at 500 K for butanoic-acid decomposition models M-1, M-2, and M-3. Figure 10 shows potential energies of the three models during the first 350 time steps of thermal annealing. Over this simulation time range, each curve decreases and ultimately approaches an asymptotic value after about 250 time steps. After 350 time steps, the potential energy of M-3 is slightly lower than M-1, but M-2 still has the highest energy. In addition, we conducted a DFT energy minimization (at 0 K) and found the same energy ordering: M-3 < M-1 < M-2, i.e., M-3 was the most stable configuration followed by M-1 (1.02 eV higher) and M-2 (5.41 eV higher than M-3). In a parallel study, DFT was used to simulate possible decompositions of ethanoic-acid on Al(111) (see Ref. 37). Ethanoic-acid is similar to butanoic-acid, i.e., it has the same functional group as that of butanoic-acid, with a shorter carbon backbone length. It was

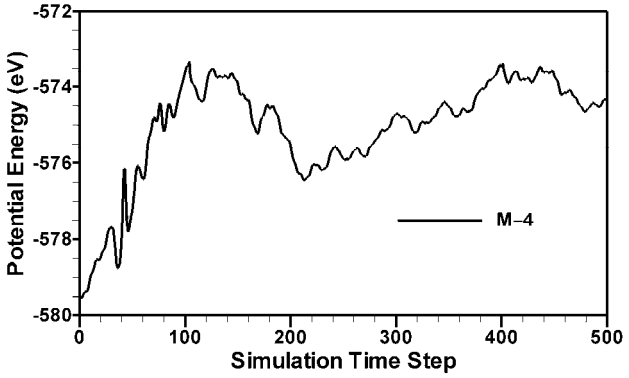

FIG. 9. Potential energy with simulation time step for butanol-alcohol decomposition on Al(111); M-4.

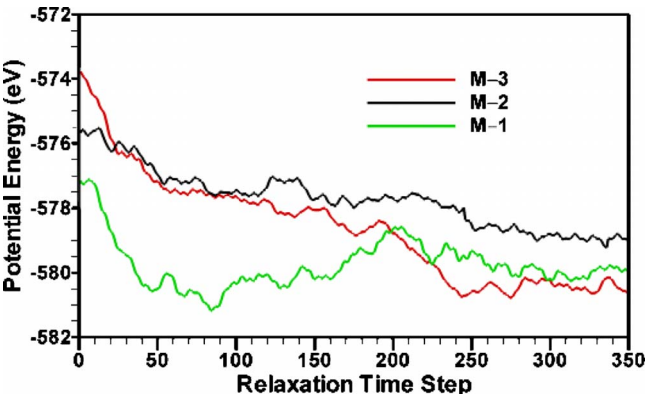

FIG. 10. (Color online) Effect of further annealing at 500 K on potential energies for butanoic-acid decomposition on Al(111). Simulation results for M-1, M-2, and M-3 are compared.

found that at very low temperatures (about 120 K), decomposition species of EA on Al(111) were attached via the alkyl-chain through the carboxyl C ion. Oxidation of the surface resulted from complete liberation of O ions from hydrocarboxyl (O=C-OH) groups on the EA molecule. This is in qualitative accord with the experimental results reported in Ref. 21.

Chen *et al.*[22,23] also carried out a comparative study for the reaction of CH_3OH with Al(111) using the same experimental methodologies. They found that CH_3OH physisorbed on the surface in a molecular conformation at 90 K. When heated up to about 143 K, a methoxy species (CH_3O) formed on Al(111). At temperatures up to 900 K, the methoxy species further decomposed, evolving $CH_4(g)$ and adsorbed C and O species on the surface.

Another experimental study[84] investigated alcohol molecules with a larger alkyl-chain than that of butanol-alcohol, including the effect of addition of oxygen-rich solvents such as H_2O. When these were added into alcohol solution, H ions were likely to dissociate from C ions before the molecule reacted with the surface due to the very large difference of electronegativity between O and H. This allowed easier liberation of oxygen from the main alkyl-chain on the alcohol molecule to oxidize the surface, plus attachment of the residual chain to the surface through its terminal C ion.

Figure 11 shows the final equilibrated configurations of decomposition species for butanoic-acid and butanol-alcohol on Al(111). Here, Fig. 11(a) represents the butanol-alcohol decomposition species in M-4. A butanol-alcoholate is adsorbed on the surface in a unidentate coordination through thermal equilibration. The dissociated H ion is adsorbed to one Al ion. Figures 11(b) and 11(c) represent butanoic-acid decompositions from models M-1 and M-3. The residual alkyl-chains anchor to the surface in tridentate coordination via their carboxyl C ions, with the OH group, and the dissociated H and O ions interacting with surface Al ions.

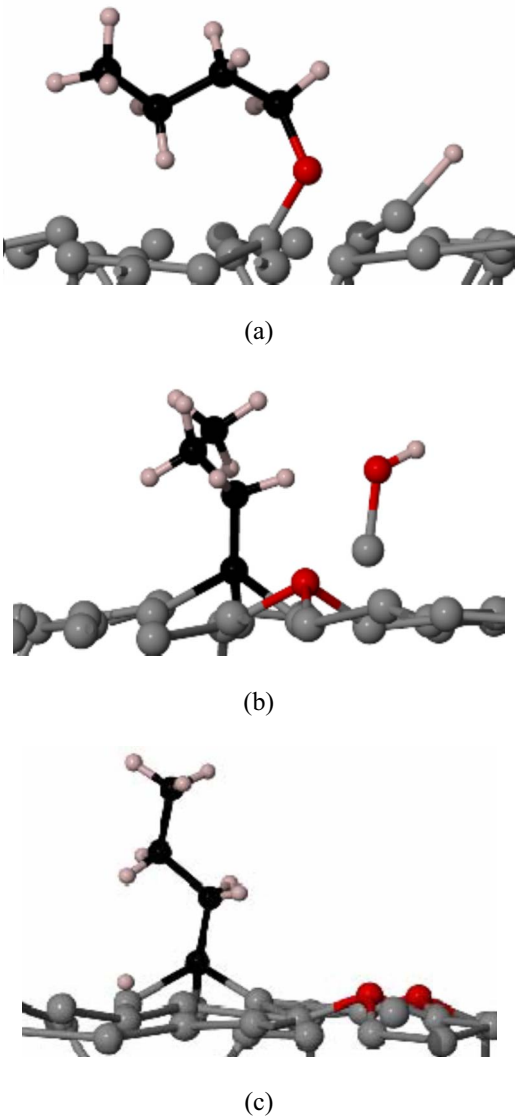

FIG. 11. (Color online) Final acid and alcohol decomposition intermediates under AIMD thermal equilibration at 500 K. (a) butanol-alcohol intermediate from M-4; (b) butanoic-acid intermediate from M-1; (c) butanoic-acid intermediate from M-3. Ion colors are red (O), black (C), white (H), and gray (Al).

E. Effect of initial molecular orientation on decomposition

The AIMD simulations were repeated in a set of ancillary calculations that explored the effect of other initial molecular orientations [relative to Al(111)] on decomposition. In the first set, the initial molecular orientations resulted from rotating those shown in Figs. 2(a), 2(c), 2(e), and 2(g) through 180°. Rather than the functional group facing the Al(111), the CH_3 end of each molecule pointed toward Al(111). In all simulations, both the butanoic-acid and butanol-alcohol molecules bounced off of Al(111) without decomposing. The Al(111) surface plane, although momentarily distorted during impact, relaxed back to a near planar configuration. By the end of each simulation, the molecules had rotated such that their functional groups were pointing toward the surface. The final vertical distances between the functional groups and the Al(111) surface plane ranged from 8–10 Å thereby precluding any further interaction. Application of another downward velocity to the rotated molecules in subsequent simulations resulted in decomposition through the molecular functional group following one of the pathways depicted in Figs. 4–6 and 8.

In the second set of ancillary AIMD simulations, the initial molecular orientations resulted from rotating those shown in Figs. 2(a), 2(c), 2(e), and 2(g) through 90° (clockwise or counterclockwise) such that the carbon backbones were aligned with the Al(111) surface plane. The butanol-alcohol molecule once again bounced off of Al(111) without decomposing. During its rebound from the surface, the molecule rotated such that its functional group was again pointing toward the surface at the end of the simulation. Interestingly, the O-H group decomposed from the butanoic-acid molecule. The remaining O ion in the fragment interacted with a surface Al ion and the carboxyl C interacted with another surface Al ion. To determine the energy of this decomposed geometry, a 500 K annealing simulation was conducted followed by a 0 K geometry optimization. A bridging configuration resulted with the O ion in the fragment inter-

acting with two surface Al ions, the carboxyl C interacting with another two surface Al ions, and the remainder of the fragment extending vertically above the surface. The final energy of the system was 2.0 eV higher than that of the M-2 decomposition suggesting that an initial 90° orientation will result in a higher energy intermediate. Similar conclusions were reached from additional AIMD calculations where the butanoic-acid molecule was rotated slightly about the axis of its carbon backbone. Based upon these additional results, we conclude that the lowest energy decomposition geometries result when the functional group of each molecule first impacts the surface. Rotation of a molecule through 90° relative to the orientations in Figs. 2, or flipping the molecule so that its CH_3 end initially impacts the surface, leads to one of two scenarios. No decomposition occurs since the molecule bounces off of the surface and ends up far enough away from the surface at the end of each simulation so as not to further interact with it. Alternatively, decomposition occurs but results in an intermediate that is higher in energy than any of those associated with the orientation in which the functional group first impacts the surface. This latter scenario applies to the butanoic-acid molecule in the initial 90° alignment and is due to its electron-rich functional group.

F. ELF analysis of butanoic-acid/Al(111)

For the four models in Fig. 2, AIMD results suggest possible bonding configurations between the molecular fragments that result from collision with Al(111). The potential-energy variations shown in Fig. 10 indicate that the binding and decomposition are energetically favorable. However, they offer no indication of electron localization upon dissociation and hence no substantive proof of bonding between the decomposed molecular species and the Al(111) slab. To provide some additional insight into bonding, we computed ELF contours in selected planes through M-1 (butanoic-acid) and M-4 (butanol-alcohol) since these result in the energetically preferred decomposition species.

Figure 12 shows computed ELF contours in a plane perpendicular to the cell *c* axis at two positions relative to the decomposed butanoic-acid fragment from M-1. The images in Figs. 12(a) and 12(b) are "tipped" so as to provide a better view of the ELF contours. We chose a configuration that is intermediate to those of Figs. 4(c) and 4(d) to best facilitate the ELF display with the ball-and-stick models that are suggestive of the decomposition species on Al(111). Figure 12(a) shows ELF contours through a subsurface layer in the Al(111) slab. The molecular fragment, which projects upward from the surface, is shown as interacting through three surface Al ions (each labeled "Al") via a C ion (labeled "C") in its backbone. The yellow-green regions intermediate to the Al sites (gray spheres that are periodically positioned in the ELF contour plane) suggest ELF ~ 0.5 which is indicative of metallic bonding in the Al. No indication of significant electron localization (or ELF ~ 0.8 or higher) is noted. Figure 12(b) shows the same slice translated (along c) into a plane between the carboxyl C ion (labeled C) and the three Al surface ions with which it interacts. The peak ELF value associated with the three contour lobes between the labeled

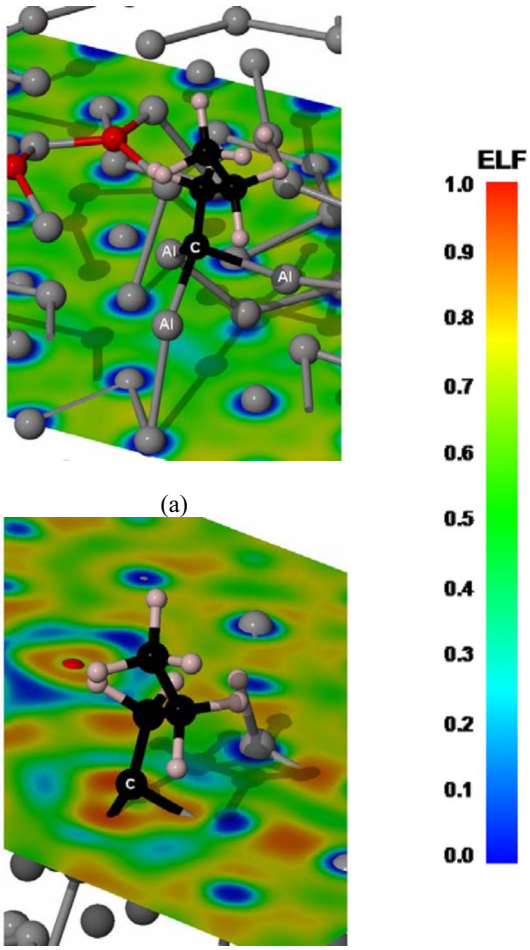

FIG. 12. (Color online) ELF contours through the same slice at two positions along the *c* axis of the simulation cell for M-1 decomposition of butanoic-acid. Carboxyl C ion is labeled C and the Al ions to which it bonds are labeled Al. (a) contour slice through subsurface Al layer suggest ELF ~ 0.5; (b) ELF=0.85 in orange portion of the contour lobes between carboxyl C ion and 3 Al surface, this denotes bonding between these species. Ion colors are red (O), black (C), white (H), and gray (Al).

C ion and the surface Al ions (these fall beneath the plane and hence are not visible in the figure) is 0.82 which is less than that in the functional group of the isolated molecule. This denotes electron localization and bonding between the butanoic-acid fragment and Al(111). The OH group is off to the left of the butanoic-acid fragment and hence is not visible in either Figs. 12(a) or 12(b). The final reaction pathway that leads to the configuration in Fig. 4(d) may be represented by the following relation:

$$H_3C\text{-}(CH_2)_2\text{-}COOH + 7Al \rightarrow H_3C\text{-}(CH_2)_2\text{-}C - 3Al + O - 3Al + H\text{-}O\text{-}Al. \quad (1)$$

Here, the decomposition products [on the right-hand side of Eq. (1)] interact (primarily) with seven Al ions. The organic fragment bonds with three Al ions as shown in Fig. 12(b). The lone O ion from the functional group of the butanoic-

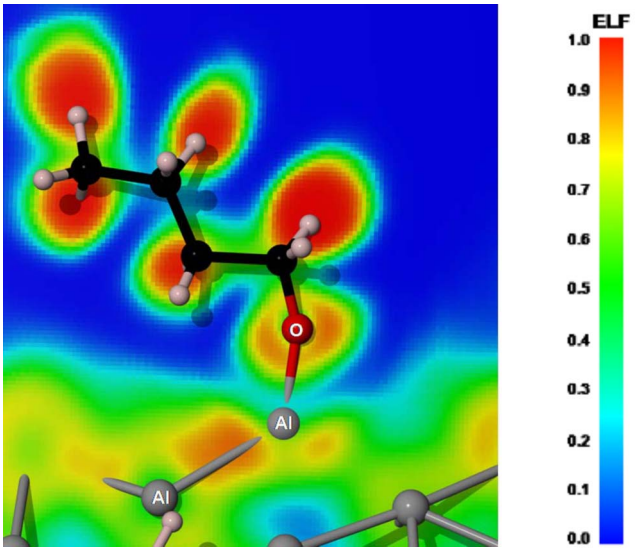

FIG. 13. (Color online) ELF contours through an oblique plane that includes the O ion (labeled "O") in the adsorbed butanol-alcohol fragment and surface Al ion immediately beneath it (labeled Al). Although the subsurface Al ion is not in the plane, the orange-red lobe between the two Al ions denotes back-bonding between the two. This results from electron transfer from the molecule to the surface. Ion colors are red (O), black (C), white (H), and gray (Al).

acid molecule interacts with three Al ions as suggested by three ELF contour lobes surrounding it in Fig. 12(b). ELF contours also confirmed that the decomposed OH group interacts with a single Al ion [not shown in Fig. 12(b)]. Note that electron localization contours (not shown in Fig. 12) suggest the following pathways for Figs. 5(d) and 6(d), respectively:

$$H_3C\text{-}(CH_2)_2\text{-}COOH + 2Al \rightarrow H_3C\text{-}(CH_2)_2\text{-}C(2O)\text{-}Al + H\text{-}Al, \quad (2)$$

$$H_3C\text{-}(CH_2)_2\text{-}COOH + 10Al \rightarrow H_3C\text{-}(CH_2)_2\text{-}C\text{-}3Al + 2(O\text{-}3Al) + H\text{-}Al. \quad (3)$$

G. ELF analysis of butanol-alcohol/Al(111)

Figure 13 shows ELF contours in an oblique plane [relative to Al(111)] that includes the O ion (red, labeled O) in the butanol-alcohol fragment and a surface Al ion (gray) immediately beneath it. The configuration shown was taken between those of Figs. 8(a) and 8(d) to facilitate the display. Of immediate note is the red-orange contour lobe between the two Al ions (a second subsurface Al ion is also labeled Al) near the bottom of the image. For this region, ELF $\sim$ 0.85, the ELF contour does not slice directly through the plane including both Al atoms (the subsurface Al ion is in front of the plane as shown). This charge localization results from electron transfer from the O ion to the Al surface and is sometimes referred to as "back bonding." This back bonding has been predicted in DFT calculations involving Al and alumina.[40] A similar, but smaller lobe can be seen to the immediate right of the Al surface ion to which is bonded the O ion. The relevant reaction pathway is given as

$$H_3C\text{-}(CH_2)_3\text{-}OH + 2Al \rightarrow H_3C\text{-}(CH_2)_3\text{-}O\text{-}Al + H\text{-}Al. \quad (4)$$

No evidence of back bonding was noted from additional ELF contours (not shown) of the decomposition configuration of butanoic-acid shown in Fig. 12.

In general, ELF analysis suggests that the alkyl-chains of the butanoic-acid and butanol-alcohol molecules are bonded to the Al surface at the conclusion of each AIMD simulation. We surmise that this will lead to the formation of effective boundary layer lubricants provided that nothing disrupts these configurations. The addition of other molecules will create additive films that cover much more of the nascent Al surface and perhaps strengthen the films through bonding interactions that run across adjacent molecular fragments. Each decomposed additive fragment can likely serve as a molecular cap (similar to the VPA molecule investigated in Ref. 37) that both lubricates the surface and possibly inhibits migration of corrosive species into the oxide surface.

VI. SUMMARY

Ab initio molecular dynamics based upon plane-wave DFT was used to explore decomposition pathways resulting from impact of single butanoic-acid and butanol-alcohol molecules on clean Al(111). The residual alkyl-chain of the butanoic-acid molecule initially reacted with Al via O ions in each of the three decomposition pathways examined. This is qualitatively consistent with experimental studies of similar reactions of other longer-chain molecules with clean Al(111). At elevated temperatures (300–500 K), the most favorable decomposition species for the butanoic-acid molecule was the attachment of the residual alkyl chain to the surface in a tridentate coordination with surface Al ions (M-1). This follows the loss of both O ions from the hydrocarboxyl (O=C-OH) group, with one in an O-H group and the other oxidizing the surface. Decomposition of the butanol-alcohol molecule was found to oxidize the surface, forming an alcoholate on the surface (in the absence of other additives). Contours of the ELF reveal electron transfer from the O ion on the molecular fragment into the Al surface and subsurface as evidenced from back bonding in the ELF contours. Additional initial molecular orientations were also explored in which the molecules were rotated through 90° and 180° relative to the Al(111) surface plane. Two scenarios resulted from these additional orientations. Either the molecules bounced off of the Al(111) without decomposing, or, in the case of the butanoic-acid with the 90° initial alignment, a higher energy decomposition intermediate resulted. The AIMD simulations therefore lead to the conclusion that the lowest energy decomposition pathways result when the functional groups of the molecules initially impact the surface.

ACKNOWLEDGMENTS

This project was sponsored by the National Science Foundation under Grant No. DMR 9619353. Computational support was provided through the NCSA Grant No. IBM-p690

at The University of Illinois at Urbana-Champaign, the Fulton High Performance Computing Center at ASU (FHPCC-ASU), and the General Motors Corporation High Performance Computing Center (IBM p6-575). The authors would like to thank N. Ooi, P. Saxe, and P.E. Krajewski for their very valuable comments on an earlier version of the manuscript. D. Stanzione, Jr. provided assistance with the Rocks Cluster at ASU.

[1] R. J. Madix, Science **233**, 1159 (1986).
[2] U. Pöschl, J. Aerosol. Med. **15**, 203 (2002).
[3] J. Wei, W. Fong, D. B. Bogy, and C. S. Bhatia, Tribol. Lett. **5**, 203 (1998).
[4] S. A. Benner, K. G. Devine, L. N. Matveeva, and D. H. Powell, Proc. Natl. Acad. Sci. U.S.A. **97**, 2425 (2000).
[5] J. F. McDermott, M. McDowell, I. G. Hill, J. Hwang, A. Kahn, S. L. Bernasek, and J. Schwarts, J. Phys. Chem. A **111**, 12333 (2007).
[6] Y. Soma and M. Soma, Environ. Health Perspect. **83**, 205 (1989).
[7] Y. Wada, Proc. IEEE **89**, 1147 (2001).
[8] M. A. Henderson, Geochim. Cosmochim. Acta **67**, 1055 (2003).
[9] G.-D. Lee, S. Han, J. Yu, and J. Ihm, Phys. Rev. B **66**, 081403(R) (2002).
[10] A. J. Dyson and P. V. Smith, Surf. Sci. **396**, 24 (1998).
[11] M. A. Phillips, N. A. Besley, P. M. W. Gill, and P. Moriarty, Phys. Rev. B **67**, 035309 (2003).
[12] W. A. Hofer, A. J. Fisher, G. P. Lopinski, and R. A. Wolkow, Phys. Rev. B **63**, 085314 (2001).
[13] Z.-X. Xie, Y. Uematsu, X. Lu, and K. I. Tanaka, Phys. Rev. B **66**, 125306 (2002).
[14] T. A. Land, R. J. Behm, J. C. Hemminger, and G. Compsa, J. Chem. Phys. **97**, 6774 (1992).
[15] N. M. D. Brown, W. J. Nelson, and D. G. Walmsley, J. Chem. Soc., Faraday Trans. 2 **75**, 32 (1979).
[16] S. DeCheveigne, S. Gauthier, J. Klein, A. Legar, C. Guinet, M. Belin, and D. DeFourneau, Surf. Sci. **105**, 377 (1981).
[17] G. Totten and H. Liang, *Surface Modification and Mechanisms: Friction, Stress and Reaction Engineering* (CRC, Cleveland, 2004).
[18] M. Sutcliffe, R. Combarieu, and P. Montmitonnet, Wear **257**, 1071 (2004); **254**, 65 (2003).
[19] S. M. Opalka, L. G. Hector, Jr., S. Schmid, and R. A. Reich, J. Tribol. **121**, 383 (1998).
[20] J. Zhong and J. B. Adams, Modell. Simul. Mater. Sci. Eng. **16**, 085001 (2008).
[21] J. E. Crowell, J. G. Chen, and J. T. Yates, Jr., J. Electron Spectrosc. Relat. Phenom. **39**, 97 (1986).
[22] J. G. Chen, J. E. Crowell, and J. T. Yates, Jr., Surf. Sci. **172**, 733 (1986); **194**, 397 (1988).
[23] J. G. Chen, J. E. Crowell, and J. T. Yates, Jr., Phys. Rev. B **33**, 1436 (1986).
[24] P. Basu, J. G. Chen, L. Ng, and J. T. Yates, Jr., J. Chem. Phys. **89**, 2406 (1988).
[25] R. Underhill and R. S. Timsit, J. Vac. Sci. Technol. A **10**, 2767 (1992).
[26] Z. Zhang, E. S. Yamaguchi, M. Kasrai, and G. M. Bancroft, Tribol. Lett. **19**, 211 (2005).
[27] M. A. Nicholls, T. Do, P. R. Nortona, G. M. Bancroft, M. Kasraia, T. W. Capehart, Y.-T. Cheng, and T. Perry, Tribol. Lett. **15**, 241 (2003).
[28] N. J. Mosey, M. H. Muser, and T. K. Woo, Science **307**, 1612 (2005).
[29] N. J. Mosey, T. K. Woo, M. Kasrai, P. R. Norton, G. M. Bancroft, and M. H. Mu, Tribol. Lett. **24**, 105 (2006).
[30] M. Koyama, J. Hayakawa, T. Onodera, K. I. Hideyuki Tsuboi, A. Endou, M. Kubo, C. A. Del Carpio, and A. Miyamoto, J. Phys. Chem. B **110**, 17507 (2006).
[31] S. Yim, N. Sonwalkar, and N. J. Saka, J. Comput.-Aided Mater. Des. **6**, 69 (1999).
[32] M. L. Greenfield and H. Ohatani, Tribol. Lett. **7**, 137 (1999).
[33] A. L. Zaitsev, F. Detraux, Y. M. Pleskachevskii, and X. Gonze, Phys. Solid State **45**, 2218 (2003).
[34] L. T. Sein, Jr. and S. A. Jansen, J. Phys. Chem. B **102**, 2415 (1998).
[35] H. Ahou, H. Tamura, S. Takami, M. Kubo, N. Zhanpeisov, and A. Miyamoto, Jpn. J. Appl. Phys., Part 1 **39**, 425 (2000).
[36] H. Zhou and H. Tamura, Appl. Surf. Sci. **158**, 38 (2000).
[37] J. Zhong and J. B. Adams, J. Phys. Chem. C **111**, 7366 (2007).
[38] L. G. Hector, Jr., S. M. Opalka, G. Nitowski, L. Wieserman, D. J. Siegel, H. Yu, and J. B. Adams, Surf. Sci. **494**, 1 (2001).
[39] http://environmentalchemistry.com/yogi/periodic/crystal.html.
[40] D. J. Siegel, L. G. Hector, Jr., and J. B. Adams, Phys. Rev. B **65**, 085415 (2002).
[41] P. Hohenberg and W. Kohn, Phys. Rev. **136**, B864 (1964).
[42] W. Kohn and L. Sham, Phys. Rev. **140**, A1133 (1965).
[43] R. Car and M. Parrinello, Phys. Rev. Lett. **55**, 2471 (1985).
[44] R. O. Jones and O. Gunnarsson, Rev. Mod. Phys. **61**, 689 (1989).
[45] M. C. Payne, M. P. Teter, D. C. Allan, T. A. Arias, and J. D. Joannopoulos, Rev. Mod. Phys. **64**, 1045 (1992).
[46] G. Kresse and J. Hafner, Phys. Rev. B **48**, 13115 (1993).
[47] G. Kresse and J. Furthmüller, Phys. Rev. B **54**, 11169 (1996).
[48] D. Vanderbilt, Phys. Rev. B **41**, 7892 (1990).
[49] P. E. Blöchl, Phys. Rev. B **50**, 17953 (1994).
[50] J. P. Perdew and Y. Wang, Phys. Rev. B **33**, 8800 (1986).
[51] J. P. Perdew, J. A. Chevary, S. H. Vosko, K. A. Jackson, M. R. Pederson, D. J. Singh, and C. Fiolhais, Phys. Rev. B **46**, 6671 (1992).
[52] G. J. Kroes, E. J. Baerends, and R. C. Mowrey, Phys. Rev. Lett. **78**, 3583 (1997).
[53] C. Tuma and J. Sauer, Chem. Phys. Lett. **387**, 388 (2004).
[54] P. Nieto, E. Pijper, D. Barredo, G. Laurent, R. A. Olsen, E.-J. Baerends, G.-J. Kroes, and Daniel Farıas, Science **312**, 86 (2006).
[55] A. Stroppa and G. Kresse, New J. Phys. **10**, 063020 (2008).
[56] S. M. Foiles, M. I. Baskes, and M. S. Daw, Phys. Rev. B **33**, 7983 (1986).
[57] Y. S. Touloukian, R. K. Kirby, R. E. Taylor, and P. D. Desai, *Thermophysical Properties of Matter* (Plenum, New York, 1975), Vol. 12.

[58] D. W. Heermann, *Computational Simulation Method in Theoretical Physics* (Springer Verlag, Berlin, 1990).
[59] S. Kojima, A. Yokoyama, M. Komatsu, and M. Kiritani, Mater. Sci. Eng., A **350**, 81 (2003).
[60] P. J. Eng, M. Newville, G. E. Brown, Jr., and G. A. Waychunas, Science **288**, 1029 (2000).
[61] E. Räsänen, A. Castro, and E. K. U. Gross, Phys. Rev. B **77**, 115108 (2008).
[62] A. Becke and K. E. Edgecombe, J. Chem. Phys. **92**, 5397 (1990).
[63] B. Silvi and A. Savin, Nature (London) **371**, 683 (1994).
[64] A. Savin, R. Nesper, S. Wengert, and T. F. Fassler, Angew. Chem. Int. Ed. Engl. **36**, 1808 (1997).
[65] P. Fuentealba, E. Chamorro, and J. C. Santos, *Understanding and Using the Electron Localization Function*, Chap. 5, in Theoretical Aspects of Chemical Reactivity, Vol. 19 (Theoretical and Computational Chemistry), edited by A. Toro-Labbé (Elsevier Science, Oxford, UK, 2007), pp. 57–86.
[66] J. C. Santos, V. Polo, and J. Andres, Chem. Phys. Lett. **406**, 393 (2005).
[67] N. H. Werstiuk and Y.-G. Wang, J. Phys. Chem. B **105**, 11515 (2001).
[68] M. Boström, Y. Prots, and Y. Grin, Solid State Sci. **6**, 499 (2004).
[69] D. Jayatilaka and D. Grimwood, Acta Crystallogr., Sect. A: Found. Crystallogr. **60**, 111 (2004).
[70] G. V. Gibbs, D. F. Cox, T. D. Crawford, M. B. Boisen, Jr., and M. Lim, Phys. Chem. Miner. **29**, 307 (2002).
[71] B. Silvi and A. Savin, Mineral. Mag. **58A**, 842 (1994).
[72] A. Savin, O. Jepsen, J. Flad, O. Andersen, H. Preuss, and H. von Schnering, Angew. Chem., Int. Ed. Engl. **31**, 187 (1992).
[73] F. Dubois, M. Schreyer, and T. F. Fassler, Inorg. Chem. **44**, 477 (2005).
[74] Y. Qi and L. G. Hector, Jr., Phys. Rev. B **69**, 235401 (2004).
[75] Y. Qi and L. G. Hector, Jr., Phys. Rev. B **68**, 201403(R) (2003).
[76] A. Savin, J. Mol. Struct. **727**, 127 (2005).
[77] Y. Sasanuma, F. Nishimura, and A. Suzuki, Langmuir **20**, 665 (2004).
[78] T. A. Olszak, F. Willig, and W. S. Durfee, Acta Crystallogr., Sect. C: Cryst. Struct. Commun. **45**, 803 (1989).
[79] R. E. Gerkin, Acta Crystallogr., Sect. C: Cryst. Struct. Commun. **53**, 1275 (1997).
[80] K. C. Hass, W. F. Schnieder, A. Curioni, and W. Andreoni, Science **282**, 265 (1998).
[81] B. K. Rao, P. Jena, S. Burkart, G. Gantefor, and G. Seifert, Phys. Rev. Lett. **86**, 692 (2001).
[82] G. E. Totten, *Handbook of Lubrication Technology* (CRC, Boca Raton, FL, 2006), Vol. 1.
[83] K. Miyoshi, B. Pohlchuck, N. C. Whittle, L. G. Hector, Jr., and J. Adams, "Properties data for adhesion and surface chemistry of aluminum. NASA Technical Publication No. TM 1998–206638, 1998 (unpublished).
[84] S. M. Opalka and L. G. Hector, Jr., Proceedings of the 220th ACS National meeting, Washington D.C., 2000, Paper No. 217.